Effective-medium theories for predicting hydrodynamic transport properties of bidisperse suspensions

Sangkyun Koo and Ashok S. Sangani

Citation: Phys. Fluids **14**, 3522 (2002); doi: 10.1063/1.1503352
View online: http://dx.doi.org/10.1063/1.1503352
View Table of Contents: http://pof.aip.org/resource/1/PHFLE6/v14/i10
Published by the American Institute of Physics.

Effective-medium theories for predicting hydrodynamic transport properties of bidisperse suspensions

Sangkyun Koo and Ashok S. Sangani[a)]
Department of Chemical Engineering and Materials Science, Syracuse University, Syracuse, New York 13244

(Received 27 December 2001; accepted 9 July 2002; published 5 September 2002)

Effective-medium theories for predicting conditionally averaged velocity field and hydrodynamic transport coefficients of monodisperse suspensions are extended to bidisperse suspensions. The predictions of the theory are shown to agree very well with the results of direct numerical simulations of bidisperse suspensions with hard-sphere configurations up to volume fractions at which phase separation in bidisperse hard-sphere systems are observed. © *2002 American Institute of Physics.* [DOI: 10.1063/1.1503352]

I. INTRODUCTION

Effective-medium theories use simple models for determining conditionally averaged fields, and hence, the effective properties of suspensions. The advances in algorithms for computing multiparticle interactions in recent years have allowed us to estimate accurately various effective properties of monodisperse suspensions, i.e., suspensions of equi-sized particles in a viscous fluid. Results for hydrodynamic transport coefficients, such as the self- and collective-mobility of the particles, the effective viscosity of the suspension, and the permeability of a fixed array of particles, determined using rigorous numerical methods (Brady and Bossis;[1] Ladd;[2] Mo and Sangani[3]) have been shown to be in good agreement with the estimates obtained using an effective-medium theory for monodisperse suspensions of spherical particles in a viscous fluid (see, e.g., Spelt *et al.*[4]). Although these numerical methods can be used to estimate the properties of bidisperse and polydisperse suspensions often encountered in practice, the results covering wide range of parameter values are not available in the literature. One of the problems in presenting the results for these suspensions is the rather large parameter space required for characterizing these suspensions. For example, for the case of bidisperse suspensions the transport coefficients must be determined as functions of the individual volume fractions and the size ratio of the particles. The spatial configurations of these suspensions may additionally depend on the nature of nonhydrodynamic interparticle forces. Thus, it is desirable to develop approximate theories that can be used to estimate hydrodynamic properties more readily than rigorous numerical simulations.[3]

The present study is concerned with the modifications that may be made to yield estimates for bidisperse suspensions, i.e., suspensions containing particles of two distinct sizes. These suspensions are encountered frequently in practice and it is not clear at the outset how the effective-medium theory that is commonly used for monodisperse suspensions may be extended to predict the properties of bidisperse suspensions. A detailed comparison of the numerical simulation results for conditionally averaged fields and various transport properties of bidisperse suspensions with those predicted by modified effective-medium theories is necessary for this purpose.

In Sec. II an effective-medium theory for monodisperse suspensions is reviewed and several possible ways of modifying it are considered to treat bidisperse suspensions. In Sec. III the results of numerical simulations for various hydrodynamic transport coefficients of bidisperse suspensions and conditionally averaged velocity fields are presented and compared with the predictions of two selected modified effective-medium theories. The simulation results are obtained by modifying the method described in Sangani and Mo.[5] It is shown that modified effective-medium theories yield reasonably accurate estimates of the hydrodynamic transport coefficients and the conditionally averaged velocities.

II. EFFECTIVE-MEDIUM THEORIES

As mentioned earlier, effective-medium theories estimate the conditionally averaged fields, and hence the effective properties of a suspension, by solving suitably averaged equations for a relatively simple model which captures some of the important multiparticle effects. The first step in developing the theory is to derive an equation for the conditionally averaged velocity and to introduce appropriate closures, and the second step is the construction of a model to evaluate the unknown constants appearing in the closures. As an example, let us consider sedimentation of equi-sized particles through a viscous fluid when the Reynolds number based on the particle radius and their average velocity is small. The suspending fluid motion satisfies

$$\frac{\partial \sigma_{ij}}{\partial x_j} + \rho_f g_i = 0, \tag{1}$$

where σ_{ij} is the stress at point $\mathbf{x}$ in the fluid, ρ_f the density of the fluid, and g_i the acceleration due to gravity. The stress

a)Telephone: 315-443-4502; fax: 315-443-2559; electronic mail: asangani@syr.edu

inside the sedimenting particle satisfies a similar equation with ρ_f replaced by the particle density ρ_p. Ensemble averaging these equations subject to the presence of a particle with its center at origin, **0**, yields

$$\frac{\partial \langle \sigma_{ij} \rangle_1}{\partial x_j}(\mathbf{x}|\mathbf{0}) + \rho(\mathbf{x}) g_i = 0, \tag{2}$$

with

$$\rho(\mathbf{x}) = \rho_f + (\rho_p - \rho_f)\langle \chi \rangle_1(\mathbf{x}|\mathbf{0}). \tag{3}$$

Here, $\chi(\mathbf{x})$ is a particle phase indicator function whose value is unity when $\mathbf{x}$ lies inside a particle and zero otherwise. The conditional average of this function may be expressed as

$$\langle \chi \rangle_1(\mathbf{x}|\mathbf{0}) = \int_{|\mathbf{x}-\mathbf{x}'| \leqslant a} P(\mathbf{x}'|\mathbf{0}) dV_{\mathbf{x}'}, \tag{4}$$

where $P(\mathbf{x}'|\mathbf{0})$ is the probability density for finding a particle with its center at $\mathbf{x}'$ given the presence of a particle at the origin. Note that $\langle \chi \rangle_1$ approaches ϕ, the volume fraction of the particles, as $r \equiv |\mathbf{x}| \to \infty$. For suspensions with an isotropic pair probability density a closure relation for the stress is introduced

$$\langle \sigma_{ij} \rangle_1 = -\langle p \rangle_1 \delta_{ij} + \mu(r)\left[\frac{\partial \langle u_i \rangle_1}{\partial x_j} + \frac{\partial \langle u_j \rangle_1}{\partial x_i}\right], \tag{5}$$

where $\langle p \rangle_1$ is the conditionally averaged pressure and $\mu(r)$ is the viscosity of the suspension. The conditionally averaged pressure and velocity are required to approach, respectively, the unconditionally averaged pressure and velocity as $r \to \infty$

$$\langle p \rangle_1 \to \langle p \rangle_0 = \rho_s g_i x_i, \quad \langle u_i \rangle_1 \to 0 \quad \text{as} \quad r \to \infty, \tag{6}$$

where $\rho_s = \rho_f + (\rho_p - \rho_f)\phi$ is the suspension density. The average sedimentation velocity of the particles equals the conditionally averaged velocity evaluated at $r = 0$.

To determine the sedimentation velocity, the above set of equations is solved for a simple effective-medium model in which $\mu(r)$ is taken to equal the suspending fluid viscosity μ_f in the exclusion region $a < r < R$ and equal to the effective viscosity μ^* of the suspension for $r > R$. Similarly, $\langle \chi \rangle_1$ is taken equal to zero in the exclusion region and equal to ϕ in the effective-medium. The exclusion radius R is chosen such that the behavior of the conditionally averaged velocity obtained from the effective-medium model agrees with its rigorous behavior as $r \to \infty$. The latter is obtained by recognizing that the apparent hydrodynamic force on the test particle at origin as ''seen'' from a large distance from the particle must balance the net force due to gravity. This apparent force obtained by integrating $(\langle \sigma_{ij} \rangle_1 - \langle \sigma_{ij} \rangle_0) n_j$ on the surface of a sphere of large radius—n_j being the unit outward normal on the surface—is given by

$$\mathbf{F}^{ap} = -(\rho_p - \rho_f) g_i \int [\langle \chi \rangle_1(\mathbf{x}|\mathbf{0}) - \phi] dV_{\mathbf{x}}. \tag{7}$$

The integral in the above equation equals the volume of the particle multiplied by the zero wave number structure factor $S(\mathbf{0})$ so that the apparent force on the particle is $S(\mathbf{0})$ times the force on the same particle in a very dilute suspension. The zero wave number structure factor is defined by

$$S(\mathbf{0}) = \int [P(\mathbf{x}|\mathbf{0}) - P(\mathbf{x})] dV_{\mathbf{x}}. \tag{8}$$

It is easy to show that the apparent force for the effective-medium model with an exclusion radius of R is given by

$$\mathbf{F}^{ap} = -(4\pi/3) g_i [\rho_p a^3 + (R^3 - a^3)\rho_f - \rho_s R^3]. \tag{9}$$

In order that the effective-medium model predicts correct behavior for the conditionally averaged stress, and hence the velocity, at large distances from the test particle, the apparent force calculated from (9) must be the same as that calculated from (7). This requires R to be given by

$$R^3 = a^3 [1 - S(\mathbf{0})]/\phi. \tag{10}$$

The results of numerical simulations for monodisperse suspensions presented by Ladd[2] and Mo and Sangani[3] correspond to hard-sphere molecular configurations. The zero wave number structure factor for the hard-sphere molecular systems is well approximated for $\phi < 0.5$ by the Carnahan–Starling approximation

$$S(\mathbf{0}) = \frac{(1-\phi)^4}{1 + 4\phi + 4\phi^2 - 4\phi^3 + \phi^4}. \tag{11}$$

Sedimentation velocity and other hydrodynamic transport properties such as the effective viscosity and the permeability of hard-sphere random suspensions have been determined by solving the Stokes flow equations rigorously (Ladd;[2] Mo and Sangani[3]). The effective-medium estimates obtained with R determined using (10) and (11) have been shown to be in very good agreement with the rigorous results (Sangani and Mo;[6] Spelt *et al.*[4]). It is natural, therefore, to extend the above method for determining R to estimate the properties of bidisperse suspensions.

Let us consider a bidisperse suspension with the particle radii a_i, densities ρ_{pi}, and volume fractions ϕ_i, $i = 1, 2$. Now the conditionally averaged stress, given that a particle of radius a_1 is centered at origin, satisfies

$$\frac{\partial \langle \sigma_{ij} \rangle_1}{\partial x_j}(\mathbf{x}|\mathbf{0}, a_1) + \left[\rho_f + \sum_{k=1}^{2} (\rho_{pk} - \rho_f)\langle \chi_k \rangle_1(\mathbf{x}|\mathbf{0}, a_1)\right] = 0, \tag{12}$$

where χ_k $(k = 1, 2)$ are the indicator functions for k-species particles. The apparent force on the particle as seen from large distances from the particle is obtained by integrating the body force term in the above expression over the entire space to yield

$$\mathbf{F}_1^{ap} = -(4\pi/3)\mathbf{g} \sum_{k=1}^{2} (\rho_{pk} - \rho_f) a_k^3 S_{k1}, \tag{13}$$

with the zero wave number structure factor defined by

$$S_{ij} = \int [P(\mathbf{x}, a_i|\mathbf{0}, a_j) - P(\mathbf{x}, a_i)] dV_{\mathbf{x}}, \tag{14}$$

where $P(\mathbf{x}, a_i|\mathbf{0}, a_j)$ is the probability density for finding a particle of radius a_i in the vicinity of $\mathbf{x}$ given that a particle

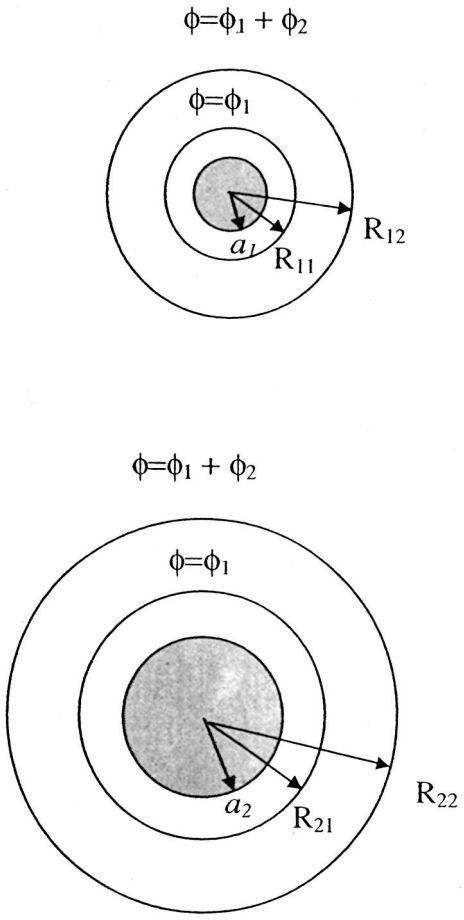

FIG. 1. A schematic representation of the effective-medium model.

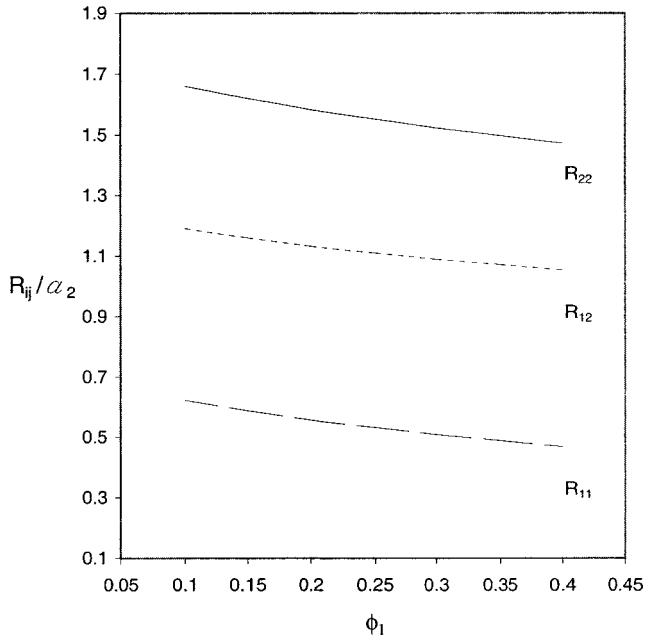

FIG. 2. R_{ij}/a_2 as a function of ϕ_1 for $\phi_2=0.1$ and $\lambda=0.5$.

of radius a_j is centered at origin and $P(\mathbf{x},a_i)$ is the (unconditional) probability density for finding a particle of radius a_i at $\mathbf{x}$.

An effective-medium model to estimate the sedimentation velocity of the particles in bidisperse suspensions consists of assuming that the particle of species 1 is centered at origin and acted upon by the gravitational force due to its mass. Outside this particle, species 1 is uniformly distributed for $r>R_{11}$ with volume fraction ϕ_1 and, likewise, species 2 for $r>R_{12}$ with volume fraction ϕ_2 (see Fig. 1). A similar model may be used to determine the conditionally averaged velocity with a particle of species 2 centered at origin. The density and the effective viscosity of the effective-medium are augmented according to the density of the particles of each species and the stresslet induced by them. In order that the apparent forces on the particles in the effective-medium model agree with the rigorous results [cf. (13)], we must choose

$$R_{ij}^3=a_i^3(\delta_{ij}-S_{ij})/\phi_i, \tag{15}$$

where δ_{ij} is the Kronecker delta function.

The above effective-medium model requires a knowledge of zero wave number structure factors S_{ij} for bidisperse suspensions. The present study will be concerned with bidisperse suspensions corresponding to bidisperse hard-sphere configurations. For very dilute bidisperse suspensions ($\phi=\phi_1+\phi_2\ll 1$) the structure factors for the hard-sphere systems can be shown easily to be given by

$$S_{ij}=\delta_{ij}-\phi_i(a_i+a_j)^3/a_i^3, \tag{16}$$

so that $R_{ij}\to a_i+a_j$ in the limit $\phi\to 0$. The structure factors for non-dilute bidisperse suspensions can be estimated using the method outlined by Ashcroft and Langreth.[7] The necessary formulas are given in Appendix A. R_{ij} decreases monotonically as the volume fraction is increased. An example is seen in Fig. 2 which shows R_{ij} for the size ratio $\lambda=a_1/a_2=0.5$ and $\phi_2=0.1$. The decrease in R_{ij} occurs due to higher probability of finding a pair of particles separated by a distance close to a_i+a_j as can be seen from Figs. 3 and 4 which show the radial distribution functions g_{11} and g_{22} for the hard-sphere bidisperse systems with $\phi_2=0.1$ at two selected values of ϕ_1. A radial distribution function g_{ij} is the pair probability density normalized by $P(a_j)$ so that its value is unity at $r=\infty$. For hard-sphere bidisperse systems these functions can be determined using the formulas given in Appendix B. The sharp rise in g_{11} at $r=2\lambda=1$ for $\phi_1=0.35$ is responsible for R_{11} to decrease to such an extent that R_{11} is, in fact, even lower than λ, the nondimensional radius of species 1. In other words, the effective-medium model for particle 1 would require that the species 1 be uniformly distributed starting from a radial distance R_{11} that is less than the radius of the particle—clearly a model that is physically meaningless. This difficulty arises whenever ϕ_1 is greater than a critical value that depends on λ and ϕ_2. Figure 5 shows this critical value for $\lambda=0.5$ and 0.7. The critical ϕ_1 is seen to decrease as ϕ_2 is increased or λ is decreased.

It is interesting to note that hard-sphere bidisperse suspensions undergo phase separation beyond a critical value of ϕ_2 for given ϕ_1 and λ. Dinsmore *et al.*[8] have carried out

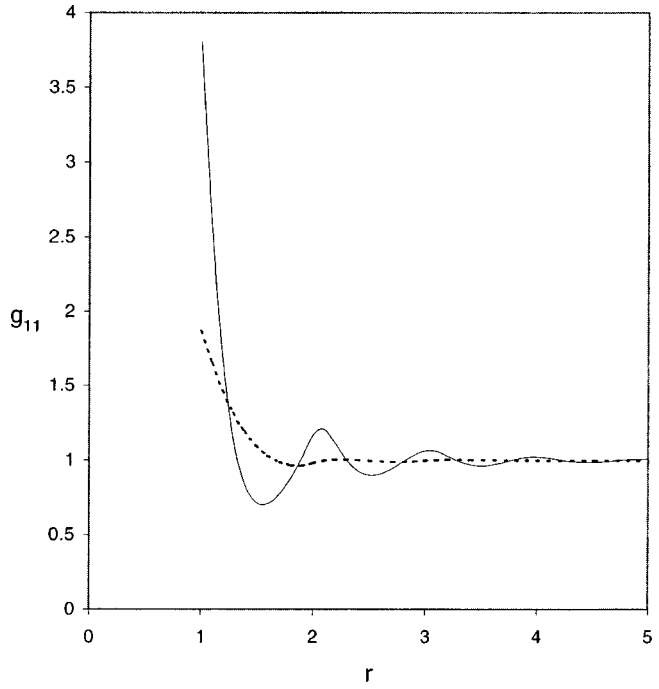

FIG. 3. Radial distribution function g_{11} at two different values of ϕ_1, 0.35 (solid line) and 0.15 (dotted line), with $\phi_2=0.1$ and $\lambda=0.5$.

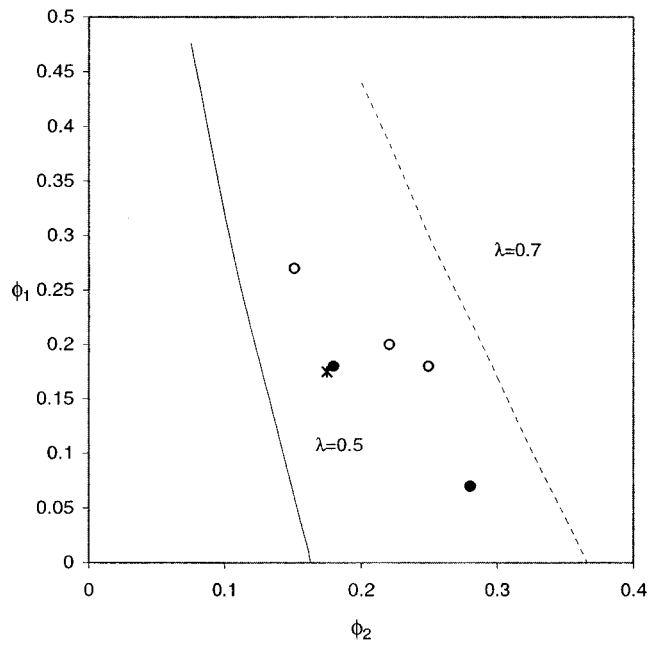

FIG. 5. The critical values of ϕ_1 as a function of ϕ_2 beyond which R_{11} becomes less than a_1 for two different size ratios: $\lambda=0.7$ and 0.5. The unfilled circles indicate the conditions where phase separation is experimentally observed and the filled circles are the conditions with no phase separation for $\lambda=0.5$ [Dinsmore *et al.* (Ref. 8)]. The star represents the conditions for which the numerical are carried out with $\phi_1=\phi_2=0.175$ and $\lambda=0.5$.

experiments with bidisperse collidal systems and observed phase separation for the conditions shown in Fig. 5. As seen from this figure the phase transition appear to occur beyond the value of ϕ_2 for which $R_{11}<a_1$.

For dense bidisperse suspensions with $R_{11}<a_1$ the effective-medium model described above cannot be used. Of course, this problem could also arise for monodisperse suspensions that have configurations other than the hard-sphere configurations examined in previous studies. Thus, we must consider other variants of the effective-medium model. It is required that the model to be chosen should satisfy the following criteria: (i) The leading order behavior of the conditionally averaged velocity at large distances from the particle must agree with its rigorous behavior; (ii) the effective properties estimated using the model should be reasonably accurate at least for the case of monodisperse suspensions; and (iii) extension to bidisperse suspensions must be natural.

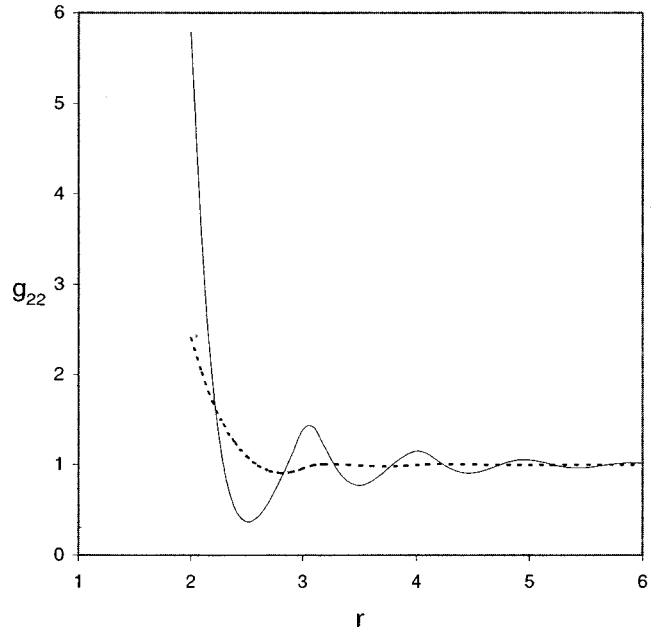

FIG. 4. Radial distribution function g_{22} at two different values of ϕ_1, 0.35 (solid line) and 0.15 (dotted line), with $\phi_2=0.1$ and $\lambda=0.5$.

The idea that the medium in the immediate vicinity of the test particle must be a clear fluid, i.e., that the properties of the medium for $a<r<R$ must be the same as that of the suspending fluid, is meaningful when the clustering of particles is not significant, or, equivalently, the radial distribution function at contact ($r=2a$) is not too large. For suspensions whose R defined by (10) is less than a, we must allow for the presence of the particles in the immediate vicinity of the test particle. Thus, a more general effective-medium model might assume that the medium immediately close to the particle corresponds to a suspension with a volume fraction ϕ_c up to radius R_c and to a suspension with volume fraction ϕ for $r>R_c$ with both ϕ_c and R_c to be specified. The condition that the apparent force on the particle be the same as given by (7) gives one relation between ϕ_c and R_c

$$\phi_c(R_c^3-a^3)=\phi(R_c^3-R^3), \tag{17}$$

where R is given by (10). Thus one may arbitrarily choose R_c and then use the above equation to estimate the volume fraction ϕ_c in the immediate vicinity of the particle. One simple choice for monodisperse suspensions is $R_c=2a$. The extension to the bidisperse suspensions will then be natural with

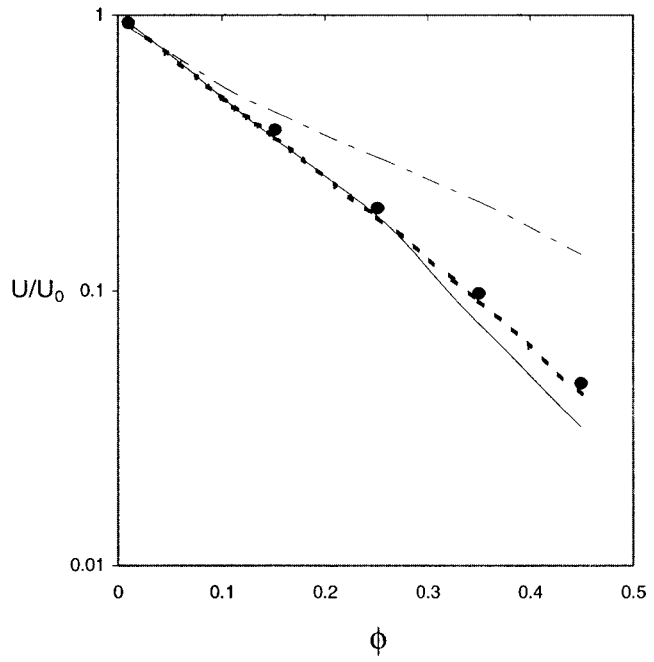

FIG. 6. Sedimentation velocity as a function of ϕ for monodisperse, hard-sphere suspensions. The thick-dotted, long-dashed, and solid lines are, respectively, the predictions by EM, EM I, and EM II theories. The filled circles indicate simulation results by Ladd (Ref. 2).

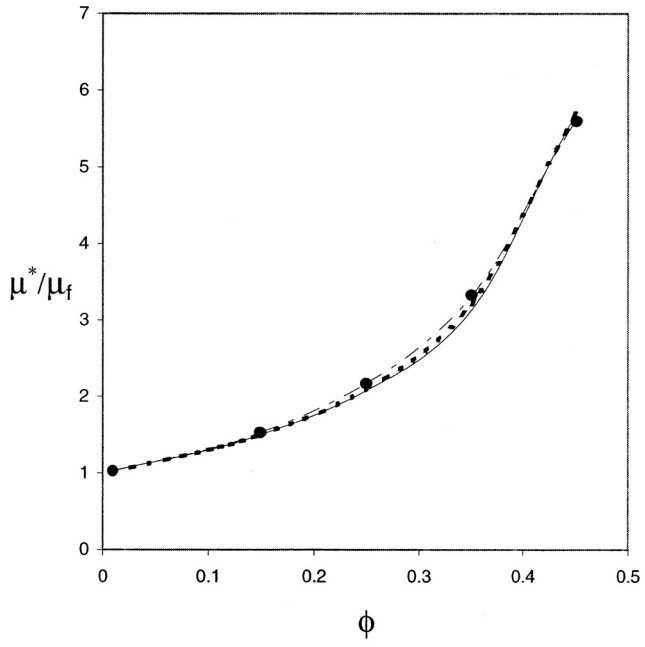

FIG. 7. Effective viscosity as a function of ϕ for monodisperse, hard-sphere suspensions. The thick-dotted, long-dashed, and solid lines are, respectively, the predictions by EM, EM I, and EM II theories. The filled triangles indicate simulation results by Ladd (Ref. 2).

$R_{c,ij}=a_i+a_j$. Equation (17) may likewise be extended to allow for the presence of the two species in the immediate vicinity of the test particle.

Unfortunately, this modified effective model (EM I) does not work as well as the original effective-medium model (EM) based on exclusion of particles for $a<r<R$ as can be seen from Figs. 6 and 7 which show the predictions of the sedimentation velocity and effective viscosity of suspensions with monodisperse, hard-sphere configurations. The circles represent the results determined using rigorous numerical simulations (Ladd[2]). At $\phi=0.45$ the nondimensional sedimentation velocity and effective viscosity are, respectively, 0.136 and 5.629 using the EM I model and 0.042 and 5.717 using the EM model, the rigorous values being 0.046 and 5.6.

The two models described above involve some arbitrary choices: EM sets the volume fraction of the particles for $a<r<R$ to *zero* while EM I sets $R_c=2a$. A model with no arbitrary choice was proposed by Chang and Acrivos in a series of papers (Acrivos and Chang;[10,11] Chang and Acrivos[9]). According to this model, henceforth to be referred to as the EM II model, the density and other properties of the medium are allowed to vary continuously. For example, the density is taken to be given by (3). Likewise, the effective viscosity of the medium is taken as

$$\mu(\mathbf{r})=\mu_f+(\mu^*-\mu_f)\langle\chi\rangle_1(\mathbf{r}|\mathbf{0})/\phi. \tag{18}$$

Here, $\langle\chi\rangle_1$ $(\mathbf{r}|\mathbf{0})$ is the conditional average of the particle volume fraction given a particle at origin as defined in (4). For suspensions in which the pair probability density is independent of the orientation of the pair, the volume integral in (4) can be reduced using simple geometrical considerations to an integration over R:

$$\langle\chi\rangle_1(r)=n\pi\int_{r-a}^{r+a}g(R)(2R-R^2/r-r+a^2/r)RdR. \tag{19}$$

Figures 6 and 7 also show predictions of sedimentation velocity and effective viscosity obtained by this model. We see that the predictions obtained by this model are better than the EM I model but not as good as those obtained by the EM model. The extension to bidisperse suspensions is straightforward for this model.

Although our primary objective in the present study is the development of effective-medium approximations for which it is sufficient to compare the results of numerical simulations for hard-sphere configurations with the predictions obtained from approximate theories, it may be noted that the numerical simulation results by Ladd[2]—and hence the theory predictions—are also in very good agreement with the experiments by Buscall *et al.*[12] for the sedimentation velocity and by van der Werff *et al.*[13] for the high-frequency effective viscosity of nearly monodisperse suspensions.

In summary, the effective-medium model based on R given by (10) gives the best estimates for the monodisperse suspensions. Its application to bidisperse suspensions, however, is limited to volume fractions for which $R_{ij}>a_j$. When this condition is not satisfied, the EM II model may be preferred to EM I or EM. Therefore, the results of numerical simulation for bidisperse suspensions will be compared with the EM and EM II models.

III. NUMERICAL METHOD

The Stokes equations of motion for monodisperse and bidisperse suspensions were solved using the method of multipole expansion outlined in Sangani and Mo[5] which uses a fast summation method that requires computational effort that scales roughly with the number of particles. The velocity induced by each particle was expressed in terms of multipoles of up to third order (i.e., $N_s=3$ in the notation of Sangani and Mo[5]). This amounts to 26 unknowns per particle. The lubrication effects require even greater values of N_s, and hence multipoles, to determine hydrodynamic transport properties accurately. Since including the lubrication effects explicitly according to the scheme outlined by Sangani and Mo[5] slows down the convergence rate of the iterative method used in the algorithm, and since modifying the method for monodisperse suspensions outlined in Sangani and Mo[5] to account for the lubrication effects in bidisperse suspensions requires considerably more effort, it was chosen to carry out calculations with greater N_s for one configuration and apply the correction obtained from the single configuration to the results obtained by $N_s=3$.

In addition to calculating the overall properties such as the sedimentation velocity and the effective viscosity, the predictions for the conditionally averaged velocity fields obtained using the effective-medium theories will be also compared with those obtained numerically. For this purpose, the velocity of the fluid or a particle at selected points in the basic unit cell was computed as described in Koch and Sangani.[14] Typically, the velocity was evaluated at 512 points, and, with N particles per unit cell, this provides $512N$ velocity versus distance from a particle data points per configuration. The conditional averaged velocity and hydrodynamic transport coefficients were obtained by averaging over 10 to 20 configurations. The number of particles N used in simulation was 1024 in most cases.

IV. EFFECTIVE-MEDIUM CALCULATIONS

The conditionally-averaged velocity and hence properties such as the sedimentation velocity, permeability, and effective viscosity were determined by solving the effective-medium equations numerically. The conditionally averaged velocity satisfies

$$\nabla\cdot\{[\mu(r)[\nabla\mathbf{u}+(\nabla\mathbf{u})^{+}]]\}+\rho(r)\mathbf{g}-\nabla p=\mu(r)\mathbf{u}/k^{*}(r), \tag{20}$$

where $\mathbf{u}$ and p are, respectively, the conditionally averaged velocity and pressure, and k^* is the Darcy permeability. The term on the right-hand side of the above equation must be used only for the case of fixed array of particles, e.g., in the calculation of permeability. For that case the viscosity to be used is Brinkman viscosity, which is taken to be the same as the fluid viscosity μ_f. For particles free to move the viscosity must be taken to be given by (18). In all calculations the mean flow was chosen such that the conditionally averaged velocity is axisymmetric around x_1-axis. Thus, it is possible to introduce a stream function to simplify the equations of motion. The stream function can be expressed as a function of r times a function of μ

TABLE I. A comparison of theoretical predictions and numerical simulation results for sedimentation velocity U nondimensionalized by the terminal velocity of an isolated sphere U_0.

		$(U/U_0)_1$			$(U/U_0)_2$		
ϕ	λ	simulation	EM	EM II	simulation	EM	EM II
0.1	0.7	0.221	0.197	0.201	0.517	0.486	0.487
0.1	0.5	0.095	0.074	0.059	0.524	0.486	0.464
0.35	0.7	0.028	0.023	0.010	0.111	0.096	0.086
0.35	0.5	−0.003		−0.014	0.116		0.092

$$\psi=f_n(r)Q_n(\mu), \tag{21}$$

where $\mu=\cos\theta$, θ being the polar angle measured from the x_1-axis, and Q_n is the integral of the Legendre function (see, e.g., Leal[15]). For determination of permeability and sedimentation velocity we take $n=1$, and that for the viscosity calculation, $n=2$. The function $f_n(r)$ must be determined by numerical integration of the equations of motion.

The above calculations apply to infinitely extended random suspensions. Numerical simulations are carried out with N particles placed in a unit cell of a periodic array. For the sedimentation and self-diffusivity problems, for which the conditionally averaged velocity decays only as $1/r$, we must account for the effect of finite N before the comparison between the two can be made. The velocity in the infinite medium due to a point force is given by

$$u_i=-\frac{F_j^{ap}}{4\pi\mu^*}\left[\delta_{ij}\frac{1}{r}-\frac{\partial^2}{\partial x_i\partial x_j}\left(\frac{r}{2}\right)\right]. \tag{22}$$

For periodic suspensions $1/r$ and $r/2$ in the above must be replaced by, respectively, spatially periodic functions S_1 and S_2 defined by Hasimoto.[16] In the numerical simulation the angular average of u_1 is computed. The angular average of S_1 and the derivatives of S_2 were determined separately and compared with the angular averages of $1/r$ and the derivatives of $r/2$ to obtain a correction factor for accounting for finite N. Accordingly, the velocity computed using the effective-medium was multiplied by the correction factor

$$C(r)=1-2.8r/h, \tag{23}$$

h being the unit cell size related to the volume fractions and radii of each particles and the number of particles.

V. RESULTS

Table I shows the results for sedimentation velocities in bidisperse suspensions. The volume fractions of the two species are equal, $\phi_1=\phi_2=\phi/2$. We see that EM provides slightly more accurate estimates than EM II. For $\phi=0.35$ and $\lambda=0.5$ the EM theory cannot be applied since $R_{11}<a\lambda$. The EM II theory predictions are in reasonable agreement with the numerical results for this case. It may be noted that the smaller particles actually move against the gravity for this case—a result that is in qualitative agreement with the EM II predictions. Figure 8 compares the predictions for the conditionally averaged velocity with those obtained numerically. We see excellent agreement in all cases with the

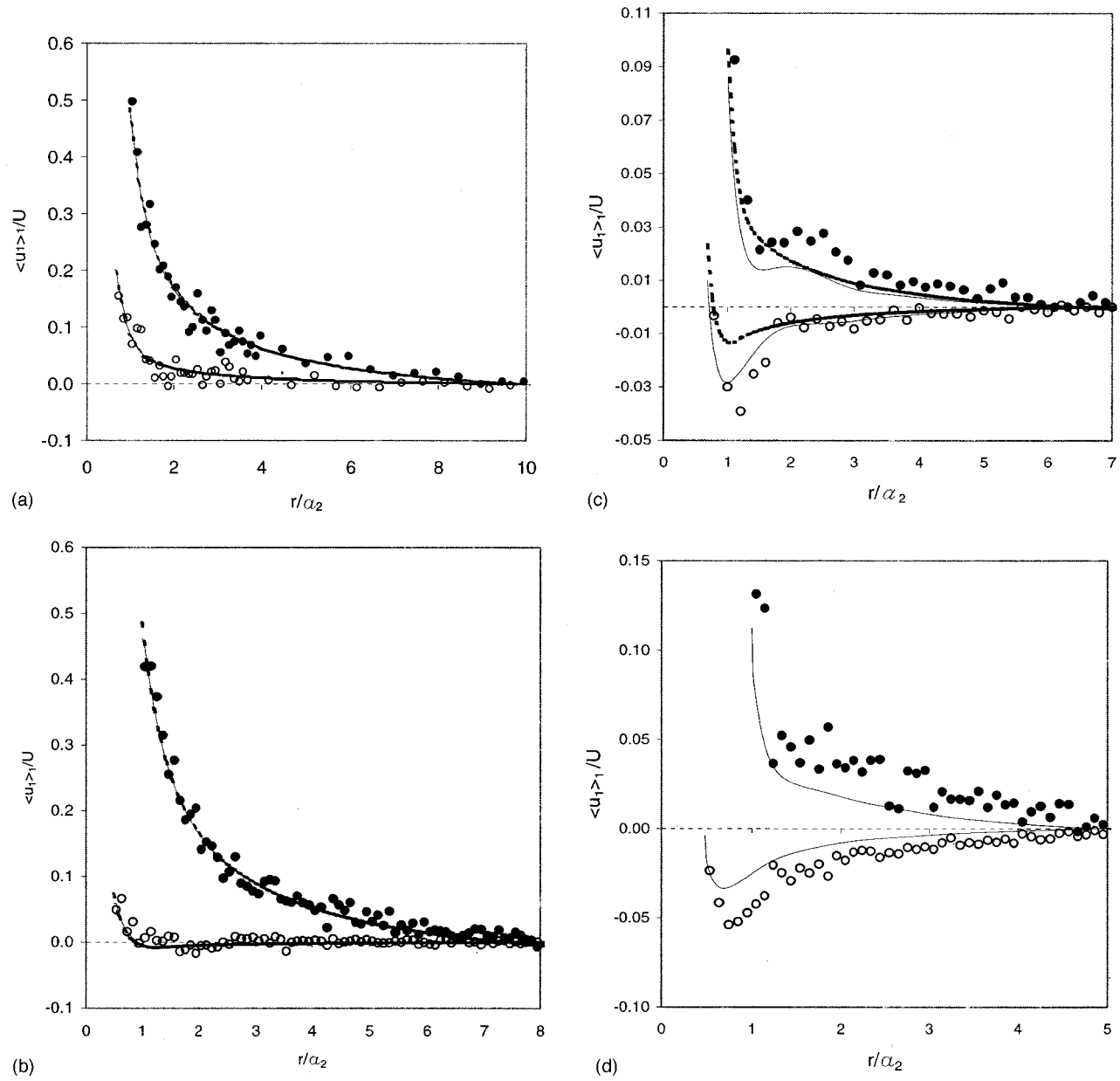

FIG. 8. A comparison of the conditionally averaged velocity $\langle u_1 \rangle_1$ nondimensionalized by superficial velocity U as a function of r from numerical simulations (filled and unfilled circles) with that from the effective-medium theories, EM (thick-dotted lines) and EM II (solid lines). The upper lines and filled circles correspond to the case when a larger sphere is at origin, and the lower lines and unfilled circles correspond to the case with a smaller sphere at origin. (a) $\phi=0.1$, $\phi_1=0.05$, and $\lambda=0.7$. (b) $\phi=0.1$, $\phi_1=0.05$, and $\lambda=0.5$. (c) $\phi=0.35$, $\phi_1=0.175$, and $\lambda=0.7$. (d) $\phi=0.35$, $\phi_1=0.175$, and $\lambda=0.5$.

predictions from both the EM and EM II models in good agreement with each other and with the data obtained from numerical simulation.

The sedimentation velocities of noncolloidal bidisperse particles have been measured by Hoyos *et al.*[17] for the size ratios of 0.6 and 0.35. The reduction in the velocity of smaller particles observed by these investigators is much smaller than the results obtained here indicating that the microstructure of sedimenting bidisperse suspensions must be significantly different from the hard-sphere microstructure for which the numerical simulations are carried out.

Table II shows results for short time self-diffusivity in bidisperse colloidal suspensions with hard-sphere spatial configurations. The short time self-diffusivity in very dilute suspensions is given by the Stokes–Einstein relation

$$D_0 = b_0 kT = \frac{kT}{6\pi\mu_f a}, \tag{24}$$

where b_0 is the mobility, defined as velocity with which a particle will move when acted upon by a force of unit magnitude, k is the Boltzmann constant, and T is the absolute temperature. To determine the short time self-diffusivity in bidisperse suspensions, a force of unit magnitude is applied to one of the particles in the suspension and its velocity is computed. The results shown in Table II were obtained by averaging over 20 numerical experiments. We see that the

TABLE II. A comparison of theoretical predictions and numerical simulation results for short time self-diffusivity D scaled by the value for very dilute suspensions D_0.

		$(D/D_0)_1$			$(D/D_0)_2$		
ϕ	λ	simulation	EM	EM II	simulation	EM	EM II
0.1	0.7	0.794	0.782	0.778	0.733	0.742	0.739
0.1	0.5	0.832	0.792	0.790	0.736	0.711	0.707
0.35	0.7	0.332	0.355	0.371	0.303	0.322	0.330
0.35	0.5	0.355		0.373	0.287		0.293

estimates by the two effective-medium theories agree with each other and that these estimates are lower than the computed values of self-diffusivities.

Table III shows the results for the effective viscosity of hard-sphere bidisperse suspensions. The effective viscosity is related to the average stresslets (Batchelor[18]) induced by the particles of each species by

$$\mu^* = \mu_f[1 + n_1 S_1 + n_2 S_2], \tag{25}$$

with the limiting values of S_j in very dilute suspensions being given by $(S_j)_0 = 10\pi a_j^3/3$. Here, n_j is the number density of the particles of species j. Once again the estimates obtained by the two effective-medium theories are in good agreement with each other and somewhat greater than the computed values of the stresslets. Comparison for the conditionally averaged velocities is shown in Fig. 9.

Wagner and Woutersen[19] and Jones[20] have determined average stresslets for dilute hard-sphere bidisperse suspensions to $O(\phi)$ using pair interactions calculations. Their analyses show that the effective viscosity of bidisperse suspensions having the same volume fraction as a monodisperse suspension is smaller and that the effective viscosity decreases as the size ratio λ decreases. The decrease, however, is generally small. For example, the effective viscosity of a monodisperse suspension with $\phi = 0.1$ is 1.300 times the suspending fluid viscosity according to the dilute theory and that for a bidisperse suspension with $\phi_1 = \phi_2 = 0.05$ and $\lambda = 0.5$ is 1.299. These estimates were obtained from the theoretical results presented by Jones.[20] These dilute theory estimates may be compared with the numerical simulations of Ladd for monodisperse suspensions which gave the effective viscosity ratio of 1.311, and the present study for bidisperse suspensions which gives for $\phi_1 = \phi_2 = 0.05$ and $\lambda = 0.5$ an effective viscosity that is 1.294 times the suspending fluid viscosity. (The results obtained in the present study were limited to a small number of configurations, and therefore, may not be accurate to third decimal place.) The dilute theory result that the viscosity of a suspension is relatively insensitive to the size ratio of particles apparently applies even to nondilute suspensions as the results in Table II would suggest. Thus, for example, the effective viscosity of suspensions with $\phi_1 = \phi_2 = 0.35/2$ and $\lambda = 0.7$ is 3.30 times the suspending fluid viscosity. The corresponding result for a monodisperse suspension with $\phi = 0.35$ is 3.33[2] and a bidisperse suspension with $\lambda = 0.5$ is 3.35.

TABLE III. A comparison of theoretical predictions and numerical simulation results for stresslet scaled by its value for very dilute suspensions.

		$S_1/(S_1)_0$			$S_2/(S_2)_0$		
ϕ	λ	simulation	EM	EM II	simulation	EM	EM II
0.1	0.7	1.170	1.185	1.166	1.193	1.213	1.129
0.1	0.5	1.154	1.180	1.126	1.200	1.222	1.228
0.35	0.7	2.499	2.494	2.302	2.763	2.628	2.496
0.35	0.5	2.470		2.281	2.904		2.649

Finally, Table IV shows the results for pressure drop in bidisperse fixed bed of particles given by

$$\nabla P = n_1 \mathbf{F}_1 + n_2 \mathbf{F}_2. \tag{26}$$

The limiting values of the force being the Stokes drag, i.e., $\mathbf{F}_{0,j} = -6\pi\mu a_j \mathbf{U}$, $\mathbf{U}$ being the superficial velocity of the fluid through the bed. We see an excellent agreement among the two theories and the simulation results. As seen in Fig. 10, the conditionally averaged velocities are also well described by the effective-medium theories.

VI. SUMMARY

The hydrodynamic transport coefficients of bidisperse suspensions depend on a relatively large number of parameters, e.g., the volume fractions of the individual species and the size ratio of the particles, and therefore, it is not practical to compute these properties and tabulate them for easy reference. Thus, simple theories that provide reasonably accurate estimates are useful. Two effective-medium theories, EM and EM II, have been considered. The former cannot be used beyond some values of the volume fraction ϕ_1 of the smaller species for given ϕ_2 and size ratio (cf. Fig. 5) for which the EM II approximation is more useful. Both theories give reasonably accurate results when ϕ_1 is less than the critical value given by Fig. 5. The effective-medium theories are shown to give quite accurate profiles of the conditionally averaged velocities in the suspensions.

ACKNOWLEDGMENTS

Financial support for this work was provided by the National Science Foundation under Grant No. CTS-9909234. The computations were performed using the resources by the National Center for Supercomputing Applications at University of Illinois at Urbana-Champaign.

APPENDIX A: STRUCTURE FACTORS FOR BINARY MIXTURES OF HARD SPHERES

Lebowitz[21] has obtained a generalized Percus–Yevick equation for determining radial distribution functions in bidisperse and polydisperse systems. For bidisperse systems the result can be expressed in the form

$$g_{ij}(r)[\exp-(\beta\varphi_{ij}(r))-1] = \exp-(\beta\varphi_{ij})C_{ij}(r), \tag{A1}$$

where $g_{ij}(r) \equiv P(\mathbf{r}, a_i | \mathbf{0}, a_j)/n_i$ is the radial distribution function, n_i being the number density of the ith species, C_{ij} is the direct correlation function representing the effect of adding a particle at a distance r from the origin in a system of $N-1$ particles with one of the particles being of radius a_j centered at origin, φ_{ij} is the pair potential, and β is a con-

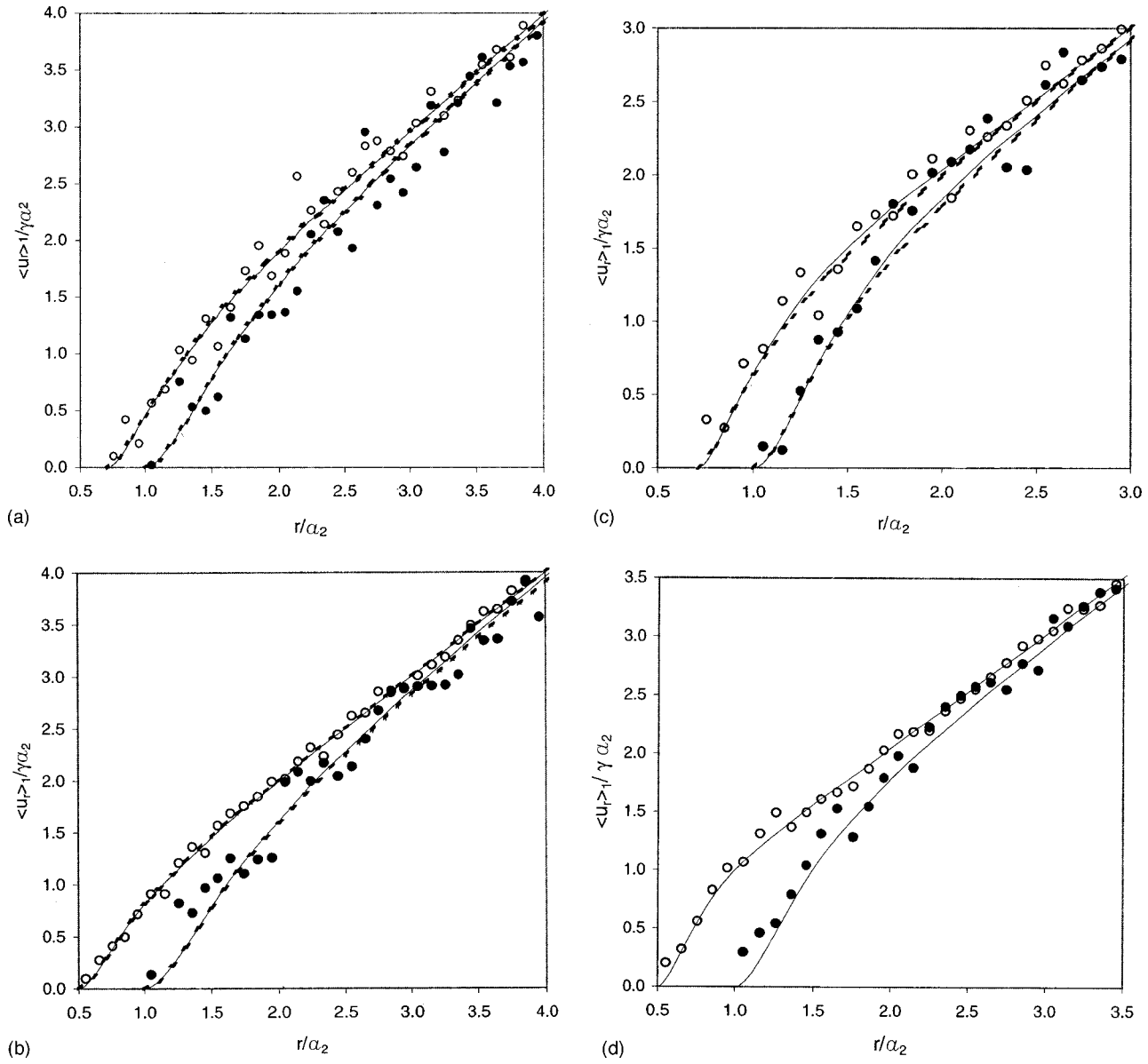

FIG. 9. A comparison of the conditionally averaged radial velocity $\langle u_r \rangle_1$, nondimensionalized by γa_2, as a function of r from numerical simulations (filled and unfilled circles) with that from the effective-medium theories, EM (thick-dotted lines) and EM II (solid lines). The lower lines and filled circles correspond to the case when a larger sphere is at origin, and the upper lines and unfilled circles correspond to the case with a smaller sphere at origin. (a) The volume fractions $\phi=0.1$, $\phi_1=0.05$, and $\lambda=0.7$. (b) $\phi=0.1$, $\phi_1=0.05$, and $\lambda=0.5$. (c) $\phi=0.35$, $\phi_1=0.175$, and $\lambda=0.7$. (d) $\phi=0.35$, $\phi_1=0.175$, and $\lambda=0.5$.

stant related to the inverse of temperature. For hard-sphere systems the pair potential is, if course, zero for $r>a_i+a_j$ and infinity otherwise. Thus, the quantity inside the square bracket on the left-hand side of the above equation vanishes for $r>a_i+a_j$ and the above equation cannot be used directly to determine g_{ij} for such values of r. Note that the direct correlation functions also vanish for $r>a_i+a_j$. Nevertheless, it is possible using the above equation as a starting point, and using the method of functional Taylor expansion, to determine both C_{ij} for $r<a_i+a_j$ and g_{ij} for $r>a_i+a_j$, as was done by Lebowitz.[21] Ashcroft and Langreth[7] showed that the structure factors are related to the Fourier transforms of the direct correlation functions. We give here the results obtained by these investigators for reader's convenience in the notation used in the present study and then specialize the results obtained to zero wave number structure factors.

TABLE IV. A comparison of theoretical predictions and numerical simulation results for drag force F scaled by the value for an isolated sphere F_0.

		$(F/F_0)_1$			$(F/F_0)_2$		
ϕ	λ	simulation	EM	EM II	simulation	EM	EM II
0.1	0.7	2.479	2.415	2.468	3.169	3.238	3.236
0.1	0.5	2.251	2.293	2.287	3.942	3.950	3.962
0.35	0.7	9.900	10.586	10.707	16.673	17.641	17.620
0.35	0.5	8.650		9.273	23.518		24.887

The direct correlation functions $C_{ij}(r)$ are given by (Lobowitz[21])

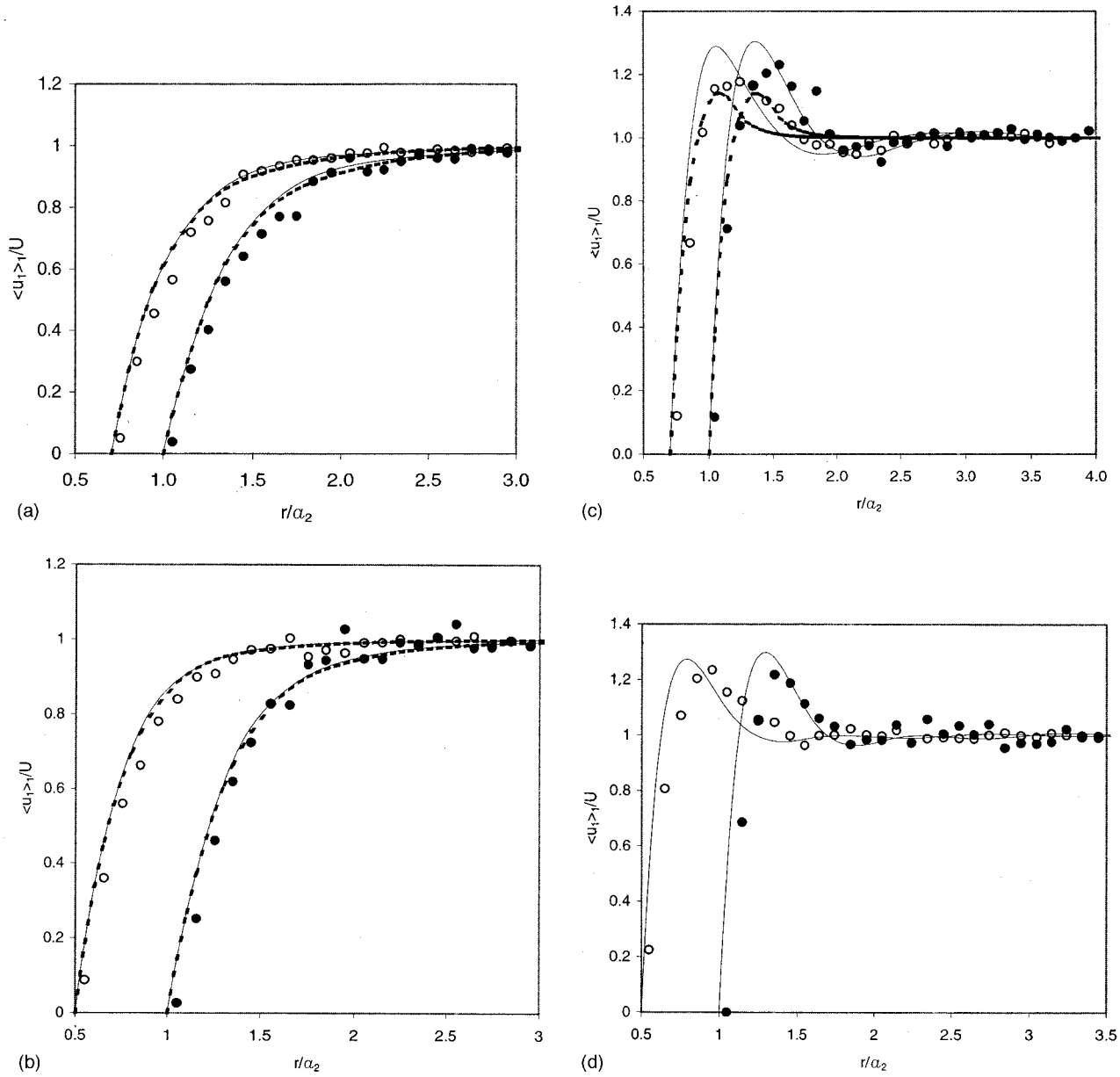

FIG. 10. A comparison of the conditionally averaged velocity $\langle u_1 \rangle_1$, nondimensionalized by superficial velocity U, as a function of r from numerical simulations (filled and unfilled circles) with that from the effective-medium theories, EM (thick-dotted lines) and EM II (solid lines). The lower lines and filled circles correspond to the case when a larger sphere is at origin whereas the upper lines and unfilled circles correspond to the case with a smaller sphere at origin. (a) $\phi=0.1$, $\phi_1=0.05$, and $\lambda=0.7$. (b) $\phi=0.1$ and $\phi_1=0.05$, and $\lambda=0.5$. (c) $\phi=0.35$, $\phi_1=0.175$, and $\lambda=0.7$. (d) $\phi=0.35$ and $\phi_1=0.175$, and $\lambda=0.5$.

$$
\begin{aligned}
-C_{11}(r) &= \alpha_1 + b_1 r + d r^3, \quad r < 2a_1, \\
-C_{22}(r) &= \alpha_2 + b_2 r + d r^3, \quad r < 2a_2, \\
-C_{12}(r) &= \alpha_1, \quad r < a_2 - a_1 \\
&= \alpha_1 + [bR^2 + 4\kappa d R^3 + dR^4]/r, \\
&\qquad a_2 - a_1 < r < a_2 + a_1,
\end{aligned}
\tag{A2}
$$

where $R=r-(a_2-a_1)$, $\kappa=a_2-a_1$, and a_1 and a_2 are the radii of small and large spheres, respectively. The coefficients α_i, b_i, b, and d are given by

$$
\alpha_1 = \frac{\partial P}{\partial \phi_1}, \quad \alpha_2 = \lambda^{-3} \frac{\partial P}{\partial \phi_2}, \tag{A3}
$$

$$
2a_1 b_1 = \beta_1 = -6[\phi_1 G_{11}^2 + \tfrac{1}{4}\phi_2 (1+\lambda)^2 \lambda G_{12}^2], \tag{A4}
$$

$$
2a_2 b_2 = \beta_2 = -6[\phi_2 G_{22}^2 + \tfrac{1}{4}\phi_1 \lambda^{-3} (1+\lambda)^2 \lambda G_{12}^2], \tag{A5}
$$

$$
2a_2 b = -3(1+\lambda)[\lambda^{-2}\phi_1 G_{11} + \phi_2 G_{22}] G_{12}, \tag{A6}
$$

$$
2a_1^3 d = \gamma_1 = \tfrac{1}{2}[\phi_1 a_1 + \lambda^3 \phi_2 a_2], \tag{A7}
$$

where $P=(\phi_1+\lambda^2\phi_2)(1+\phi+\phi^2)-3\phi_1\phi_2(1-\lambda)^2[1+\phi_1+\lambda(1+\phi_2)](1-\phi)^{-3}$ and G_{11}, G_{22}, and G_{12} are the radial distribution functions at $r=2a_1$, $2a_2$, and $a_{12}=a_1+a_2$, respectively,

$$G_{11}=[(1+\tfrac{1}{2}\phi)+\tfrac{3}{2}\phi_2(\lambda-1)](1-\phi)^{-2},$$
$$G_{22}=[(1+\tfrac{1}{2}\phi)+\tfrac{3}{2}\phi_1(\lambda^{-1}-1)](1-\phi)^{-2}, \tag{A8}$$
$$G_{12}=\left[\left(1+\frac{1}{2}\phi\right)+\frac{3}{2}\frac{1-\lambda}{1+\lambda}\phi_1(\phi_1-\phi_2)\right](1-\phi)^{-2}.$$

As mentioned above Ashcroft and Langreth[7] showed that the Fourier transform of the correlation functions are related to the structure factors. Their results can be specialized to zero wave numbers to yield

$$S_{11}(0)=\left\{1-n_1\hat{C}_{11}(0)-\frac{n_1n_2\hat{C}_{12}^2(0)}{1-n_2\hat{C}_{22}(0)}\right\}^{-1},$$
$$S_{22}(0)=\left\{1-n_2\hat{C}_{22}(0)-\frac{n_1n_2\hat{C}_{12}^2(0)}{1-n_1\hat{C}_{11}(0)}\right\}^{-1},$$
$$S_{12}(0)=n_1^{1/2}\hat{C}_{12}(0)\{[1-n_1\hat{C}_{11}(0)]\times[1-n_2\hat{C}_{22}(0)]-n_1n_2\hat{C}_{12}^2(0)\}^{-1}, \tag{A9}$$
$$S_{21}(0)=n_2^{1/2}\hat{C}_{12}(0)\{[1-n_1\hat{C}_{11}(0)]\times[1-n_2\hat{C}_{22}(0)]-n_1n_2\hat{C}_{12}^2(0)\}^{-1}.$$

Here, $\hat{C}_{ij}(0)$ are the Fourier transforms of the direct correlation functions in the limit of zero wave numbers

$$-n_1\hat{C}_{11}(0)=24\phi_1\left\{\frac{\alpha_1}{3}+\frac{\beta_1}{4}+\frac{\gamma_1}{6}\right\},$$
$$-n_2\hat{C}_{22}(0)=24\phi_2\left\{\frac{\alpha_2}{3}+\frac{\beta_2}{4}+\frac{\gamma_1}{6\lambda^3}\right\}, \tag{A10}$$
$$-n_1^{1/2}n_2^{1/2}\hat{C}_{12}(0)=\frac{\phi x^{1/2}(1-x)^{1/2}}{x+(1-x)\lambda^3}\left\{\alpha_1(1-\lambda)^3 24\lambda^3\times\left[\frac{1-\lambda}{2\lambda}\left(\frac{\beta_{12}}{3}+\frac{\gamma_{12}}{4}+\frac{\gamma_1}{5}\right)+\frac{\beta_{12}}{4}+\frac{\gamma_{12}}{5}+\frac{\gamma_1}{6}+\alpha_1\left(\frac{1}{3}+\frac{1-\lambda}{4\lambda}+\frac{1-\lambda}{4\lambda^2}\right)\right]\right\},$$

where

$$x=\frac{n_2}{n_1+n_2},$$
$$\gamma_{12}=2\gamma_1\frac{1-\lambda}{\lambda}, \tag{A11}$$
$$\beta_{12}=-3\lambda(1+\lambda)(\lambda^{-2}\phi_1G_{11}+\phi_2G_{22})G_{12}.$$

Note that β_1, β_2, and γ_1 are given in the expressions for b_1, b_2, and d, respectively [cf. (A4), (A5), and (A7)].

APPENDIX B: RADIAL DISTRIBUTION FUNCTIONS FOR BINARY MIXTURES OF HARD SPHERES

Lebowitz[21] has given expressions for the radial distribution functions g_{ij} for binary mixtures of hard spheres by solving the generalized Percus–Yevick equation. His solutions for g_{ij} are given in terms of their Laplace transforms. These need to be inverted to determine g_{ij} as functions of r for the purpose of calculations based on EM II theory. Throop and Bearman[22] have used a numerical method for inverting the Laplace transforms. Later, Leonard *et al.*[23] provided an explicit expression for g_{ij} using the inversion procedure described by Throop and Bearman.[22] However, the formulas given by these later investigators are incorrect.

We, therefore, followed the calculation procedure for $g_{ij}(r)$ given by Throop and Bearman.[22] The inversion integrals of the Laplace transforms for $g_{ij}(r)$ are given by

$$rg_{11}(r)=\frac{1}{12\xi_1}\sum_{m=0}^{\infty}\frac{1}{2\pi i}\int\frac{s[H-L_2(s)\exp(2sa_2)][I(s)]^m\exp[s(r-2a_1-2a_2)]ds}{[F(s)]^{m+1}},$$
$$rg_{22}(r)=\frac{1}{12\xi_2}\sum_{m=0}^{\infty}\frac{1}{2\pi i}\int\frac{s[H-L_1(s)\exp(2sa_1)][I(s)]^m\exp[s(r-2a_1-2a_2)]ds}{[F(s)]^{m+1}}, \tag{B1}$$
$$rg_{12}(r)=\sum_{m=0}^{\infty}\frac{1}{2\pi i}\int\left(\left[12(\xi_2a_2^3-\xi_1a_1^3)(a_2-a_1)-a_{12}\left(1-\frac{1}{2}\phi\right)\right]s-(1+2\phi)\right)\frac{[I(s)]^ms^2\exp[s(r-a_{12})]ds}{[F(s)]^{m+1}},$$

where $\xi_i=\pi n_i/6$, n_i being the number density of species i. H, $L_1(s)$, $L_2(s)$, $F(s)$ and $I(s)$ are given by

$$H=72\xi_1\xi_2(a_2-a_1),$$
$$L_1(s)=12\xi_2[(1+\tfrac{1}{2}\phi)+12\xi_1a_1^2(a_2-a_1)]a_2s^2+[12\xi_2(1+2\phi)-2Ha_1]s+H,$$
$$L_2(s)=12\xi_1[(1+\tfrac{1}{2}\phi)+12\xi_2a_2^2(a_1-a_2)]a_1s^2+[12\xi_1(1+2\phi)-2Ha_2]s+H, \tag{B2}$$

$$F(s)=H+[12(\xi_1+\xi_2)(1+2\phi)-2H(a_1+a_2)]s-72(\xi_1a_1^2+\xi_2a_2^2)^2s^2-24(\xi_1a_1^2+\xi_2a_2^2)(1-\phi)s^3-(1-\phi)^2s^4,$$

$$I(s)=L_2(s)\exp(-2sa_1)+L_1(s)\exp(-2sa_2)-H\exp[-2s(a_1+a_2)].$$

The integrals in (B1) can be expressed as equal to $2\pi i R_m^{ij}$ using the residue theorem where

$$R_m^{ij}=\frac{1}{(m-1)!}\sum_{t_i}\lim_{s\to t_i}\left(\frac{d^{m-1}}{ds^{m-1}}[(s-t_i)^m]\times\sum_{k=1}^{2}\frac{\varphi_k^{ij}(s)\exp(s[r-\psi_k^{ij}(a_1,a_2)])}{[F(s)]^m}\right), \tag{B3}$$

where t_i correspond to the four roots of $F(s)=0$. Here, φ_k^{ij} are polynomials in s and are given by

$$\varphi_1^{11}=\frac{-L_2(s)s}{12\xi_1}\Xi(s),\quad \varphi_2^{11}=\frac{Hs}{12\xi_1}\Xi(s),$$

$$\varphi_1^{22}=\frac{-L_1(s)s}{12\xi_2}\Xi(s),\quad \varphi_2^{22}=\frac{Hs}{12\xi_2}\Xi(s), \tag{B4}$$

$$\varphi_1^{12}=\left\{\left[12(\xi_2a_2^3-\xi_1a_1^3)(a_2-a_1)-a_{12}\left(1-\frac{1}{2}\phi\right)\right]s-(1+2\phi)\right\}s^2\Xi(s),$$

$$\varphi_2^{12}=0,$$

$$\text{where}\quad \Xi(s)=\sum_{q_1=0}^{q_1+q_2}\sum_{q_2=0}^{+q_3=}\sum_{q_3=0}^{m-1}\frac{(m-1)!}{q_1!q_2!q_3!}\times L_2(s)^{q_1}L_1(s)^{q_2}(-H)^{q_3}.$$

ψ_k^{ij} are linear combinations of a_1 and a_2

$$\psi_1^{11}=2(m-q_2)a_1+2(m-q_1-1)a_2,$$

$$\psi_2^{11}=2(m-q_2)a_1+2(m-q_1)a_2,$$

$$\psi_1^{22}=2(m-q_2-1)a_1+2(m-q_1)a_2, \tag{B5}$$

$$\psi_2^{22}=2(m-q_2)a_1+2(m-q_1)a_2,$$

$$\psi_1^{12}=2(m-q_2-\tfrac{1}{2})a_1+2(m-q_1-\tfrac{1}{2})a_2,\quad \psi_2^{12}=0.$$

Now $g_{ij}(r)$ can be determined by carrying out the differentiation in (B3). Since the contour integrals in (B1) equal the sum of the residues R_m^{ij} for $r-\psi_k^{ij}(a_1,a_2)>0$ and are zero otherwise, the evaluation of g_{ij} as a function of r is limited by the differentiation order m. Calculation of $g_{ij}(r)$ at large r requires higher order differentiation which becomes quite cumbersome. In the present study, the differentiation was carried out up to $m=4$ which is sufficient to determine g_{ij} for $r<8a_1+2a_i$. Beyond this distance, $g_{ij}(r)$ was taken to be unity in our calculations.

[1] J. F. Brady and G. Bossis, "Stokesian dynamics," Annu. Rev. Fluid Mech. **20**, 111 (1988).
[2] A. J. C. Ladd, "Hydrodynamic transport coefficients of random dispersions of hard spheres," J. Chem. Phys. **93**, 3484 (1990).
[3] G. Mo and A. S. Sangani, "A method for computing Stokes flow interactions among spherical objects and its application to suspensions of drops and porous particles," Phys. Fluids **6**, 1637 (1994).
[4] P. D. M. Spelt, M. Norato, A. S. Sangani, M. S. Greenwood, and L. L. Tavlarides, "Attenuation of sound in concentrated suspensions: Theory and experiments," J. Fluid Mech. **430**, 51 (2001).
[5] A. S. Sangani and G. Mo, "An O(N) algorithm for Stokes and Laplace interactions of particles," Phys. Fluids **8**, 1990 (1996).
[6] A. S. Sangani and G. Mo, "Elastic interactions in particulate composites with perfect as well as imperfect interfaces," J. Mech. Phys. Solids **45**, 2001 (1997).
[7] N. W. Ashcroft and D. C. Langreth, "Structure of binary liquid mixtures. I," Phys. Rev. **156**, 685 (1967).
[8] A. D. Dinsmore, A. G. Yodh, and D. J. Pine, "Phase diagrams of nearly hard-sphere binary colloids," Phys. Rev. E **52**, 4045 (1995).
[9] E. Chang and A. Acrivos, "The rate of heat conduction from a heated sphere to a packed bed of passive spheres," Chem. Eng. Commun. **58**, 165 (1987).
[10] A. Acrivos and E. Chang, "The transport properties of nondilute suspensions. Renormalization via an effective continuum method," AIP Conf. Proc. Vol. 154, *Physics and Chemistry of Porous Media II*, edited by J. R. Banavar, J. Koplik, and K. W. Winkler (American Institute of Physics, New York, 1987), p. 129.
[11] A. Acrivos and E. Chang, "A model for estimating transport quantities in two-phase materials," Phys. Fluids **29**, 3 (1986).
[12] R. Buscall, J. W. Goodwin, R. H. Ottewill, and T. F. Trados, "The settling of particles through Newtonian and non-Newtonian media," J. Colloid Interface Sci. **85**, 78 (1982).
[13] J. C. van der Werff, C. G. de Kruiff, C. Blom, and J. Mellema, "Linear viscoelastic behavior of dense hard-sphere dispersions," Phys. Rev. A **39**, 795 (1989).
[14] D. L. Koch and A. S. Sangani, "Particle pressure and marginal stability limits for a homogeneous gas fluidized bed: Kinetic theory and numerical simulations," J. Fluid Mech. **400**, 229 (1999).
[15] L. G. Leal, *Laminar Flow and Convective Transport Processes: Scaling Principles and Asymptotic Analysis* (Butterworth-Heinemann, Boston, 1992).
[16] H. Hasimoto, "On the periodic fundamental solutions of the Stokes equations and their application to viscous flow past a cubic array of spheres," J. Fluid Mech. **5**, 317 (1959).
[17] M. Hoyos, J. C. Bacri, J. Martin, and D. Salin, "A study of the sedimentation of noncolloidal bidisperse, concentrated suspensions by an acoustic technique," Phys. Fluids **6**, 3809 (1994).
[18] G. K. Batchelor, "The stress system in a suspension of force-free particles," J. Fluid Mech. **41**, 545 (1970).
[19] N. J. Wagner and A. T. J. M. Woutersen, "The viscosity of bimodal and polydisperse suspensions of hard spheres in the dilute limit," J. Fluid Mech. **278**, 267 (1994).
[20] R. B. Jones, "High-frequency viscosity of a dilute polydisperse colloidal suspension," Physica A **212**, 43 (1994).
[21] J. L. Lebowitz, "Exact solution of generalized Percus–Yevick equation for a mixture of hard sphere," Phys. Rev. **133**, A895 (1964).
[22] G. J. Throop and R. J. Bearman, "Radial distribution functions for mixtures of hard spheres," J. Chem. Phys. **42**, 2838 (1965).
[23] P. J. Leonard, D. Henderson, and J. A. Barker, "Calculation of the radial distribution function of hard sphere mixtures in the Percus–Yevick approximation," Mol. Phys. **21**, 107 (1971).